Journal of Alloys and Compounds 508 (2010) 364–369

Contents lists available at ScienceDirect

Journal of Alloys and Compounds

journal homepage: www.elsevier.com/locate/jallcom

Study on $Pb(Mg_{1/3}Ta_{2/3})O_3$–$Pb(Mn_{1/3}Sb_{2/3})O_3$–$Pb(Zr_xTi_{1-x})O_3$ high power piezoelectric ceramics near the morphotropic phase boundary

Yu Cheng[a], Ying Yang[b,*], Yiping Wang[b], Hanqi Meng[a]

[a] College of Materials Science and Technology, Nanjing University of Aeronautics and Astronautics, 29 Yudao Street, Nanjing 210016, China
[b] Precision Driving Laboratory, Nanjing University of Aeronautics and Astronautics, 29 Yudao Street, Nanjing 210016, China

ARTICLE INFO

Article history:
Received 19 December 2009
Received in revised form 6 August 2010
Accepted 6 August 2010
Available online 18 August 2010

Keywords:
Ferroelectrics
Piezoelectric ceramics
High power
Morphotropic phase boundary

ABSTRACT

$Pb(Mg_{1/3}Ta_{2/3})O_3$–$Pb(Mn_{1/3}Sb_{2/3})O_3$–$Pb(Zr_xTi_{1-x})O_3$ quaternary piezoelectric ceramics with different compositions near the morphotropic phase boundary were synthesized using a conventional solid state reaction method. The phases, microstructures, ferroelectric, piezoelectric and dielectric properties of the system were investigated. A transition from rhombohedral to tetragonal phase was observed as the Zr/Ti ratio decreased. The *P–E* loops presented pinched shapes at low electric fields and the distortions disappeared at high electric fields. The dielectric study revealed a diffuse phase transition behavior in the ceramics. The optimal dielectric and piezoelectric properties $\varepsilon_r = 817$, $d_{33} = 285$ pC/N, $k_p = 0.55$, $T_C = 302\,^\circ$C, $\tan\delta = 0.4\%$ and $Q_m = 1600$ of the ceramics were obtained at the composition of Zr/Ti = 50/50. Vibration velocity at $\Delta T = 20\,^\circ$C was found as high as 0.74 m/s for this composition, which was almost 2.5 times as that of the commercial hard PZT ceramics.

1. Introduction

Ultrasonic motors, used as compact servomotors for precision positioning, have many advantages over the conventional electromagnetic motors, and are currently widely used in aeronautics, astronautics, and medical applications [1]. Piezoelectric materials used in ultrasonic motors are electrically driven to high mechanical vibration near the resonance frequencies, leading to a temperature rising and deterioration of piezoelectric properties with the increase of their vibration velocities. Therefore, piezoelectric materials are necessary to have high mechanical quality factor (Q_m) [2–4]. Moreover, high piezoelectric coefficient (d_{33}) and electromechanical coupling factor (k_p) are also required for high torque output and efficiency. For piezoelectric properties enhancement, $Pb(Zr,Ti)O_3$ (PZT) based ternary or quaternary systems, such as PZN–PZT [5], PMN–PZT [6], PMN–PZN–PZT [7], PMN–PFW–PZT [8], have been intensively investigated. It is reported that in these systems, ceramics with compositions near the morphotropic phase boundary (MPB) always possess optimum properties. For example, perovskite-structured $Pb(Mg_{1/3}Ta_{2/3})O_3$–$Pb(Zr,Ti)O_3$ (PMgT–PZT) ceramics with compositions near MPB show a dielectric constant (ε_r) and a piezoelectric coefficient of the order of 4000 and 580 pC/N respectively. However, the Q_m of this system is only 70 [9]. On the other hand, the ternary system $Pb(Mn_{1/2}Sb_{2/3})O_3$–$Pb(Zr,Ti)O_3$ (PMS–PZT) presents excellent hard properties, Q_m value of 1755 has been reported in this system under proper sintering conditions [10].

In our previous work, we introduced $Pb(Mg_{1/3}Ta_{2/3})O_3$ into PMS–PZT to form a quaternary system and good properties were obtained [11]. But the piezoelectric properties near the MPB of this system are still not clear. It is well known that the MPB of PZT lies in the region of Zr/Ti ratio around 53/47, but in some ternary or quaternary systems, doping ions will lead to slight shift of the MPB [12]. Therefore, in this study, the effects of Zr/Ti ratio on the structure and electrical properties of the system $Pb(Mg_{1/3}Ta_{2/3})O_3$–$Pb(Mn_{1/3}Sb_{2/3})O_3$–$Pb(Zr_xTi_{1-x})O_3$ (PMgT–PMS–PZT) was investigated in order to obtain the MPB composition of this system.

In high power devices, such as ultrasonic motors, the used piezoelectric materials usually endure high vibration velocity and large deformation. Thus, measurements under low vibration level may not appropriate to evaluate the performance in high-vibration conditions. Therefore, many investigations have been focused on the high-power properties of the piezoelectric ceramics [13,14]. In our study, the high-power properties of the ceramics near the MPB were also evaluated.

2. Experimental procedures

Ceramics of $0.05Pb(Mg_{1/3}Ta_{2/3})O_3$–$0.05Pb(Mn_{1/3}Sb_{2/3})O_3$–$0.9Pb(Zr_xTi_{1-x})O_3$, where $x = 0.56$, 0.54, 0.52, 0.50, 0.48, and 0.46, were synthesized by a conventional solid-state reaction method. Pb_3O_4 (99.5%), MgO (4N), Ta_2O_5 (4N), MnO_2 (99.95%), Sb_2O_3 (99.5%), ZrO_2 (4N) and TiO_2 (99%) were weighed stoichiometrically, with 0.5 wt% excess Pb_3O_4 to compensate the lead loss during sintering. The starting

* Corresponding author. Tel.: +86 25 84891937; fax: +86 25 84893075.
E-mail address: yingyang@nuaa.edu.cn (Y. Yang).

0925-8388/$ – see front matter © 2010 Elsevier B.V. All rights reserved.
doi:10.1016/j.jallcom.2010.08.026

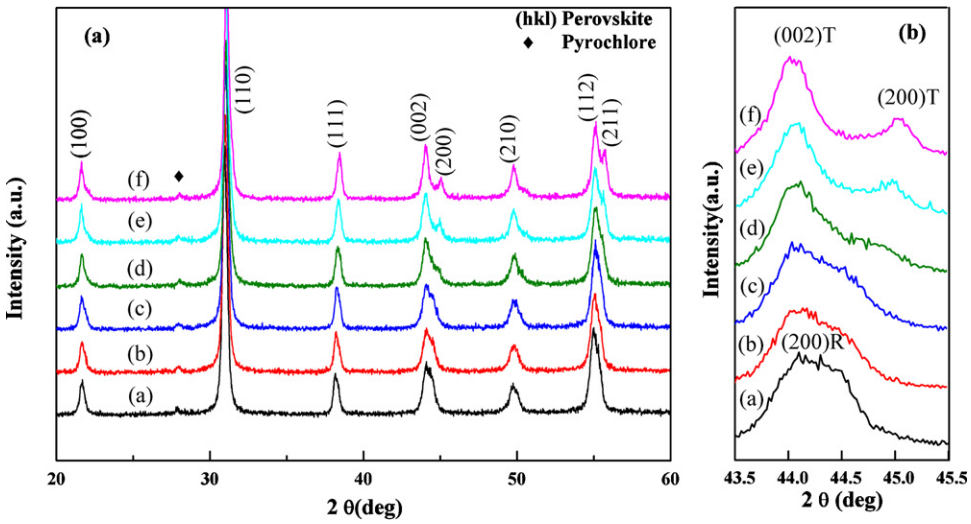

Fig. 1. XRD patterns of 0.05PMgT–0.05PMS–0.9PZT ceramics with different Zr/Ti ratios: (a) Zr/Ti = 56/44; (b) Zr/Ti = 54/46; (c) Zr/Ti = 52/48; (d) Zr/Ti = 50/50; (e) Zr/Ti = 48/52; (f) Zr/Ti = 46/54.

powders were wet-milled for 16 h in ethanol and then the mixtures were dried and calcined at 850 °C for 2 h. The calcined powders were pulverized again for 20 h. With the addition of polyvinyl alcohol (PVA, 5 wt%) as a binder, the ground powders were pressed into pellet samples under uniaxial pressure of 250 MPa. Sintering was carried out at 1240 °C for 2 h in sealed alumina crucibles with the samples covered by their original powders to minimize lead loss. Next, the sintered pellets were cut into 0.8 mm in thickness and printed with silver electrodes on both sides. Electroded samples were subsequently fired at 550 °C for 20 min and poled in silicon oil under a 4 kV/mm electric field for 30 min at 120 °C. The electrical properties of the samples were measured 24 h after poling.

The bulk densities of the sintered samples were measured by the Archimedes method, and all the densities are verified higher than 7.7 g/cm^3. The crystal structures of the sintered samples were analyzed by using an X-ray diffractometer (Bruker D8 Advanced, Cu Kα radiation, λ = 0.15418 nm). For the microstructure observation, the samples were thermally etched at 1150 °C for 15 min and examined by scanning electrical microscopy (SEM, Quanta 200, FEI Company). Piezoelectric measurements were made using a quasi-static piezo-d_{33} meter (ZJ-3A, Institute of Acoustics Academic Sinica). The dielectric constant and loss (tan δ) were measured in the temperature range from room temperature to 600 °C and the frequency range from 1 kHz to 1 MHz by utilizing an impedance analyzer (Agilent 4294A) with a laboratory heating device. Planar coupling coefficient and mechanical quality factor were determined by the resonance and anti-resonance frequencies. Ferroelectric hysteresis loops were obtained at room temperature using a ferro-analyzer (TF2000, aixACCT GmbH). The vibration velocity υ was measured using a Doppler Laser Vibrometer (Polytec PSV-300F, Germany), during which the temperature rise was determined by a infrared radiation thermometer (Victor 303, China).

3. Results and discussion

3.1. Crystal structure and microstructure

Fig. 1(a) shows the XRD patterns of the PMgT–PMS–PZT ceramics. All the samples present a perovskite structure with minor pyrochlore phase. Meanwhile, the broadening and splitting of the (2 0 0) peak can be seen from fine scans of 2θ between 43° and 46° with the decrease of Zr/Ti ratio (Fig. 1(b)). When the Zr/Ti ratio is greater than 50/50, only one single (2 0 0)R peak is observed. At the Zr/Ti ratio of 48/52, the single peak splits into double peaks of (0 0 2)T and (2 0 0)T, indicating a transition from rhombohedral to tetragonal phase induced by the variation of Zr/Ti ratio. The MPB of this system is around Zr/Ti ratio of 48/52. In PZT based binary ceramics, MPB lies in the region of Zr/Ti ratio around 53/47. When doping ions such as Ta^{5+} (0.64 Å), Mg^{2+} (0.72 Å), Mn^{2+} (0.67 Å) and Sb^{5+} (0.6 Å) dissolve into the crystal lattice, they usually substitute B sites of the perovskite structure and lead to a change in lattice constants and shift the MPB. This phenomenon was also observed in other PZT-based systems [12].

The variation of lattice constants with decrease of the Zr/Ti ratio is shown in Fig. 2. The *a*-axis and the *c*-axis are equal to each other and show little change when the Zr/Ti ratio is greater than 50/50. The lattice is indexed as a rhombohedral structure. As the Zr/Ti ratio decreases, the *c*-axis ascends while the *a*-axis descends consistently, which indicates that the tetragonality of the structure is enhanced.

Fig. 3 presents the SEM micrographs of PMgT–PMS–PZT ceramics with different Zr/Ti ratios. All of them show a dense microstructure with few pores. The observation agrees well with the high density measured by the Archimedes method. A few small diamond-shaped grains with dimensions of about 0.5–1 μm along with the relatively large grains of 1–3 μm dimensions can be observed. The grain size does not vary noticeably with different Zr/Ti ratios. The compositions of these grains were examined by X-ray energy dispersive spectroscopy (EDS). It is found that the contents of Sb and Ta elements in the small grains are much higher than that of the large grains. It is probably because the diffusion of these two elements with high atom weight is hard during the sintering process. Therefore a few small grains with rich contents of these two elements are formed in some regions.

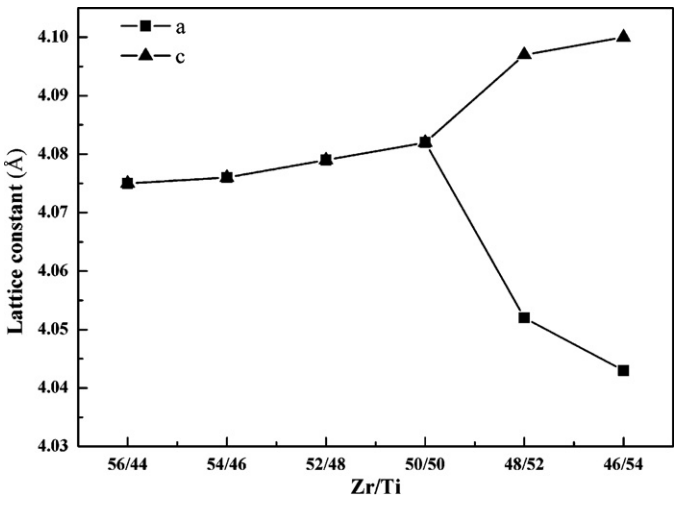

Fig. 2. Lattice constants of PMgT–PMS–PZT ceramics with different Zr/Ti ratios.

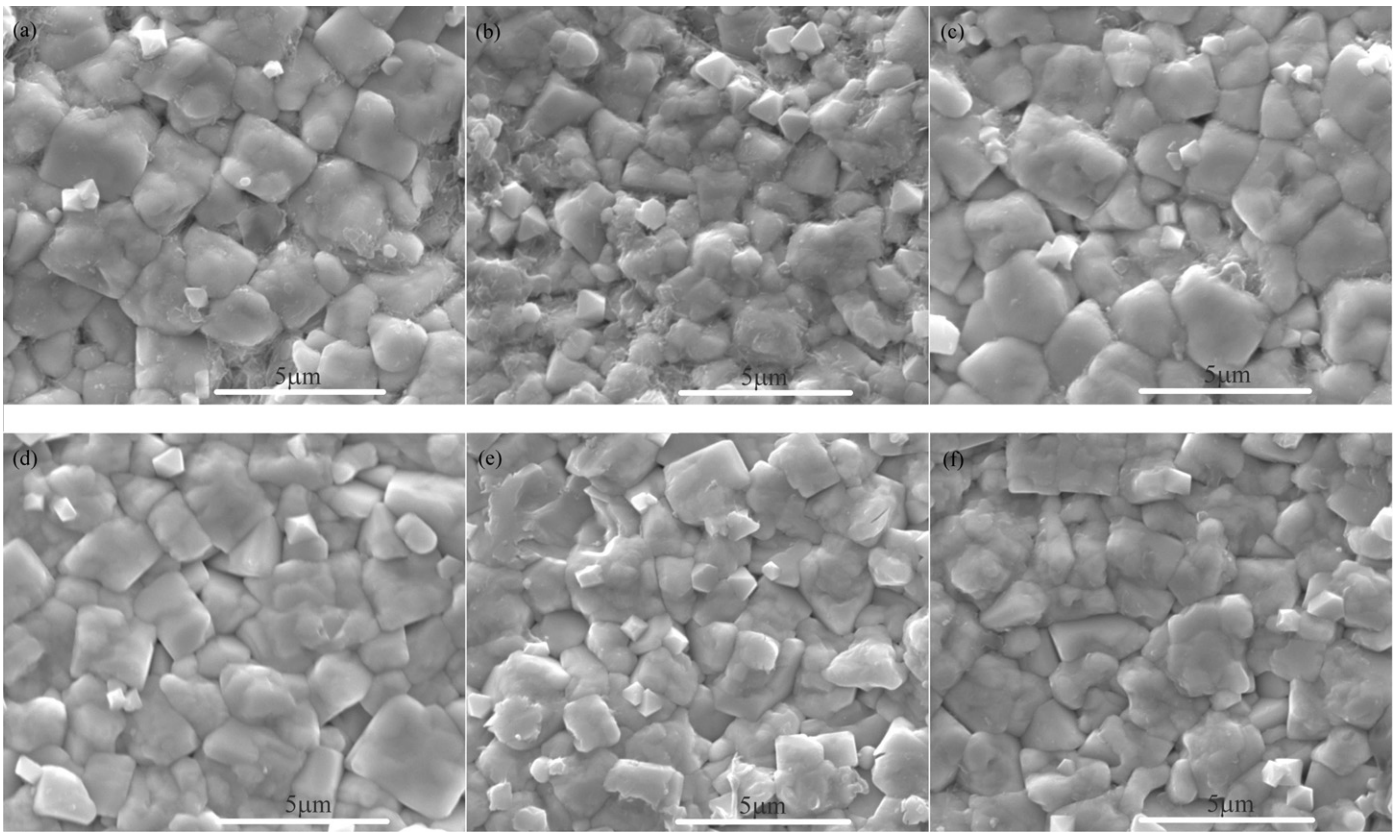

Fig. 3. SEM micrographs of the thermally etched surfaces of PMgT–PMS–PZT ceramics: (a) Zr/Ti = 56/44; (b) Zr/Ti = 54/46; (c) Zr/Ti = 52/48; (d) Zr/Ti = 50/50; (e) Zr/Ti = 48/52; (f) Zr/Ti = 46/54.

3.2. Ferroelectric characteristics

Fig. 4(a) exhibits the polarization-electric field (*P–E*) loops for 0.05PMgT–0.05PMS–0.9PZT ceramics with Zr/Ti = 56/44 at different electric fields. It is interesting to see that the *P–E* curve shows a pinched shape at low electric field. When the electric field is higher than 5.8 kV/mm, the distortion in hysteresis loops disappears and the polarization increases to saturation. Various mechanisms have been proposed to explain the observed pinched shape. Carl and Hardtl attributed the pinched hysteresis loops to an internal bias field and observed the disappearance of the distortion hysteresis loop in PZT after repeated cycling [15]. Some researchers suggested that the pinched shape was probably related to defect dipoles formed by combination of oxygen vacancies with doped ions at B-sites, which acted as pinning points for the domain motion and resulted in a constricted loop [16,17]. Zhang et al. observed pinched shape of *P–E* loops in $Pb(Mn_{1/3}Nb_{1/3}Sb_{1/3})_x(Zr_{0.825}Ti_{0.175})_{1-x}O_3$ and they proved the existence of oxygen vacancies by X-ray photoelectron spectroscopy (XPS). They also assumed that the pinched shape results from the pinning effect of the defect dipoles [18].

Since all the hysteresis loops are symmetric under low or high electric fields, the pinched shape could not arise from the internal bias field. Thus, it is attributed to the defect dipoles that act as pinning points for the domain motions. When Ta^{5+}, Sb^{5+}, Mn^{2+} and Mg^{2+} ions with high valences got into B-sites to substitute Zr^{4+} and Ti^{4+}, to maintain the electric neutrality, oxygen vacancies were formed under the condition that they were not fully compensated by lead vacancies. The oxygen vacancies and the B-site ions form defect dipoles and result in an abnormal behavior of *P–E* loop. When the electric field is below 4.2 kV/mm, it is not strong enough to overcome the pinning effect caused by the defect dipoles, so that domains of the ceramics cannot be fully switched. At the electric field of 6 kV/mm, the dipoles are substantially rotated by the field, hence they do not constrict the domains anymore and normal hysteresis loops are obtained.

Fig. 4(b) presents the *P–E* loops for 0.05PMgT–0.05PMS–0.9PZT ceramics with different Zr/Ti ratios under a saturated electric field and a frequency of 50 Hz. The inset of Fig. 4(b) shows the composition dependence of remnant polarization (P_r) and coercive field (E_c) of 0.05PMgT–0.05PMS–0.9PZT ceramics. It is found that the evaluated P_r value increases initially and then decreases when the Zr/Ti ratio decreases. The maximum value of P_r of 9.18 μC/cm^2 is reached at Zr/Ti = 50/50, where rhombohedral phase predominates near MPB compositions. In bulk $Pb(Zr_xTi_{1-x})O_3$ ceramics [19,20] and other quaternary ceramics, such as $Pb(Zr_xTi_{1-x})O_3$–$Pb(Mn_{1/3}Nb_{2/3})O_3$–$Pb(Zn_{1/3}Nb_{2/3})O_3$ (PZT–PMN–PZN) [21], it has also been reported that P_r exhibits a highest value at MPB. It can be ascribed to the fact that the phase coexistence offers more polarization near MPB [19–21]. However, these values of P_r and the dependence of P_r on composition are quite different from those of bulk PZT single crystals and single-crystal PZT films, where P_r was proved to have the lowest value both theoretically [22] and experimentally [23]. It has been believed that this difference may arise since the P_r of PZT based ceramics depends primarily on the ease with which the sample can be poled and not the intrinsic single-crystal value of P_r [23]. Meanwhile, E_c increases a little when the Zr/Ti ratio decreases.

3.3. Dielectric and piezoelectric properties

The dependences of dielectric and piezoelectric properties on the Zr/Ti ratio at room temperature are illustrated in Fig. 5. It can be seen that ε_r, $\tan\delta$, d_{33} and k_p increase initially and reach their maximum values at Zr/Ti = 0.48/0.52 and then decrease. The maxima of

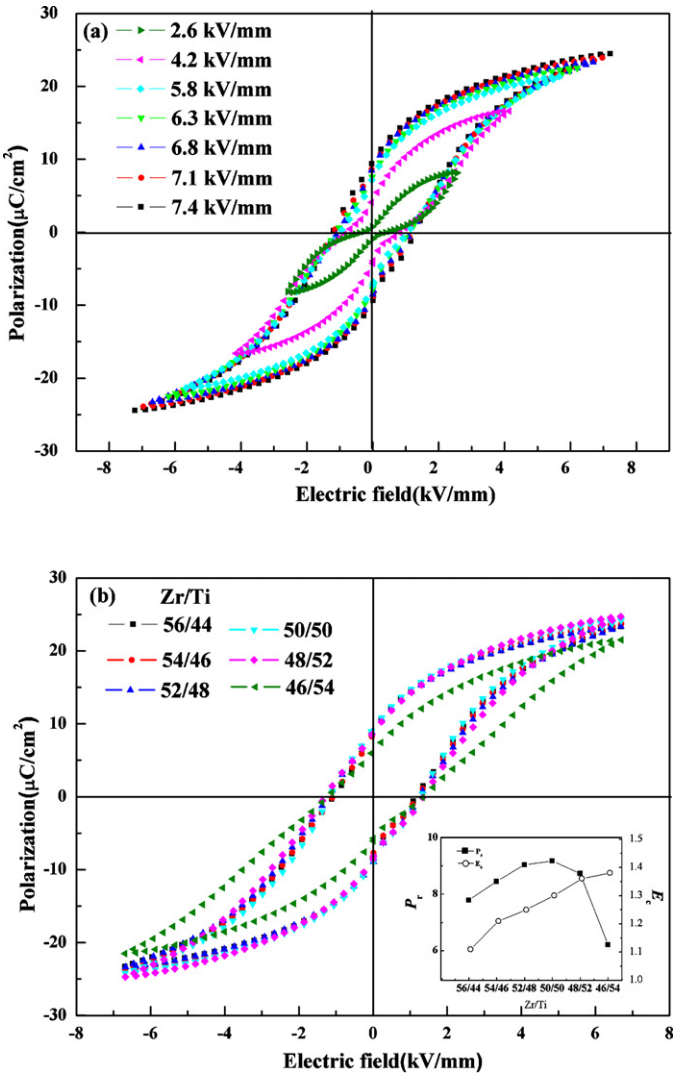

Fig. 4. *P–E* loops of PMgT–PMS–PZT piezoelectric ceramics: (a) *P–E* loops of sample with Zr/Ti = 56/44 at different electric fields from 2.6 kV/mm to 7.4 kV/mm and (b) *P–E* loops of samples with different Zr/Ti ratios under saturated driven field; the inset shows the composition dependence of P_r and E_c.

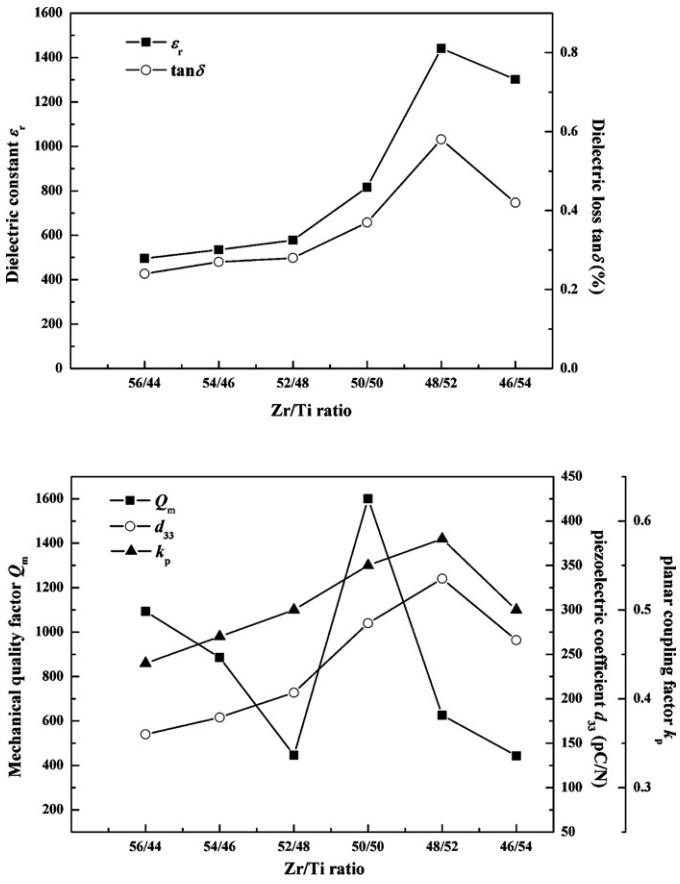

Fig. 5. Dielectric and piezoelectric properties of PMgT–PMS–PZT ceramics as a function of Zr/Ti ratio.

ε_r, d_{33} and k_p are 1441, 335 pC/N, 0.58, respectively. The trend is similar with the composition dependence of the remnent polarization, probably because of the same reasons. It has been reported that as Zr/Ti changes, the phase transition made the mechanical strain preserve one phase against the other relaxed, which caused the peak in the dielectric constant as a function of composition and also led to the maximum electro-mechanical response [24,25]. On the other hand, the spontaneous polarization of the rhombohedral phase can be oriented in any of its eight crystallorgraphic directions as well as in any of the six crystallographic directions in the tetragonal phase. The tetragonal phase and the rhombohedral phase coexist at the MPB composition, the spontaneous polarization can be oriented along all of these available 14 directions and it is beneficial to domain motions in poling, resulting in high dielectric and piezoelectric properties [25]. However, the piezoelectric property Q_m does not change regularly. It decreases with decrease of the Zr/Ti ratio initially and then jumps to a maximum value of 1600 at the Zr/Ti ratio of 50/50. While further decrease the Zr/Ti ratio, the value decreases again. The initial decrease in Q_m can be ascribed to the increase of internal friction. As the composition closes to MPB, the spontaneous polarization directions increase and the domain walls are easier to move under the driving electric field, which always leads to the increase of the internal friction of the ceramics and the decrease of Q_m. Microstructure is another important aspect that affects Q_m. From the SEM micrographs, it can be seen that the ceramic with Zr/Ti ratio of 50/50 has a dense structure and uniform grains. Consequently, the ceramic of this composition possesses the maximum Q_m value.

The variation of dielectric constant ε_r at 1 kHz frequency as a function of temperature of the ceramics with different Zr/Ti ratios is shown in Fig. 6(a). The measurements confirm that the Curie temperature (T_C) increases from 286 °C to 304 °C with Zr/Ti changing from 56/44 to 46/54, which is similar to PZT. $PbZrO_3$ has a Curie temperature of 230 °C while $PbTiO_3$ has a high Curie temperature of 490 °C. The Curie temperature increases as the tetragonality of the ceramics increases. In this quaternary system, the dependence of the Curie temperature on the Zr/Ti ratio can also due to the phase transition. The maxima of dielectric constants were in the range of 13,000–17,000. The composition with Zr/Ti = 50/50 shows the highest dielectric constant peak. Fig. 6(b) presents the temperature dependence of the dielectric constant ε_r of samples of Zr/Ti ratio of 50/50 under various frequencies from 1 kHz to 1 MHz. A diffuse phase transition with strong frequency dispersion has been observed in this sample and other compositions. The peak dielectric constant decreases as the frequency increases, while the peak position does not change markedly. For quantitative estimation for the diffuse phase transition of the ferroelectrics, the dielectric constant can be described according to a modified Curie–Weiss formula:

$$\frac{1}{\varepsilon_r} - \frac{1}{\varepsilon_m} = \frac{(T - T_m)^\gamma}{C} \quad (1)$$

where ε_m is the maximum dielectric constant and T_m is the corresponding temperature. γ and C are constants depending on the

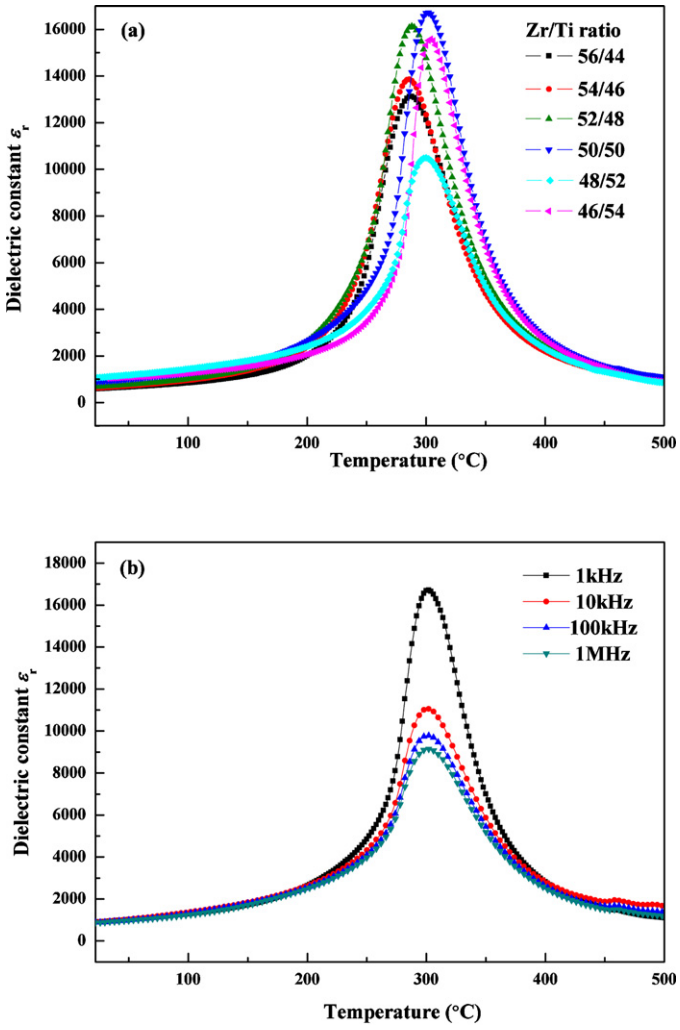

Fig. 6. (a) ε_r as a function of temperature of PMgT–PMS–PZT ceramics with different Zr/Ti ratios and (b) ε_r as a function of temperature and frequency of the composition with Zr/Ti = 50/50.

characteristics of the samples. The value of γ indicates phase transition characteristics of the sample. For $\gamma = 1$, it refers to the normal Curie–Weiss law; when $\gamma = 2$, it describes a complete diffuse phase transition [26]. Fig. 7 shows the plot of $\ln(1/\varepsilon_r - 1/\varepsilon_m)$ as a function of $\ln(T - T_m)$ at 1 kHz for 0.05PMgT–0.05PMS–0.9PZ$_x$T$_{1-x}$ ceramics. The values of γ are calculated from the slopes in Fig. 7 by linear fitting. The γ value increases from 1.70 at Zr/Ti = 56/44 to 1.74 at Zr/Ti = 50/50 and then decreases with further decrease of the Zr/Ti ratio. It is generally accepted that the relaxor behavior arises from a frustration of long-range ferroelectric coupling due to the localized disorder in the crystal structure [27]. When the Zr/Ti ratio decreases from 56/44 to 46/54, the structure of the sample experience a transition from rhombohedral phase to tetragonal phase, and the maximum γ value is obtained at the composition of Zr/Ti = 50/50, which possesses the highest degree of disorder.

3.4. High-power properties

For a circular sample driven under the k_p mode, the maximum vibration velocity (υ_m) is shown as follows [28]:

$$\upsilon_m = \sqrt{\frac{\varepsilon_{33}^T}{2\rho(1+\sigma)}}\frac{Bk_pQ_mV_m}{T} \quad (2)$$

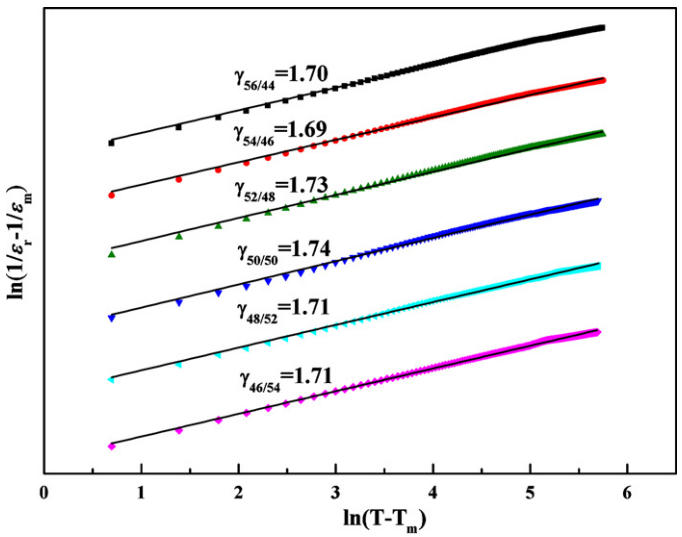

Fig. 7. $\ln(1/\varepsilon_r - 1/\varepsilon_m)$ as a function of $\ln(T - T_m)$ at 1 kHz for PMgT–PMS–PZT ceramics with different Zr/Ti ratios [symbols: experimental data; solid lines: fitting to Eq. (1)]

where ε_{33}^T is the relative permittivity, B is a constant with the value of 2.065, k_p is the planar coupling coefficient, Q_m is the mechanical quality factor, V_m is the maximum applied AC voltage, ρ is the density of sample, σ is the Poission ratio and T is the thickness of the sample.

To observe the high-power properties of the ceramics, compositions with Zr/Ti = 52/48 and 50/50 were chosen to test under high voltage. Fig. 8 shows the relationship between the vibration velocity and the electric field (E) of the two compositions. It can be seen that the vibration velocity is nearly proportional to the electric field and the highest velocities of both compositions are higher than 0.7 m/s. Under the same electric field, the velocity of the sample with Zr/Ti = 50/50 is higher than that of the sample with Zr/Ti = 52/48.

Above a certain vibration velocity, the increase in temperature (ΔT) under electrical driving is significant. This restricts the practical upper limitation for υ_m. For high-power devices, a high υ_m and simultaneously a low heat generation during performance are desired. From the practical perspective, the maximum vibration

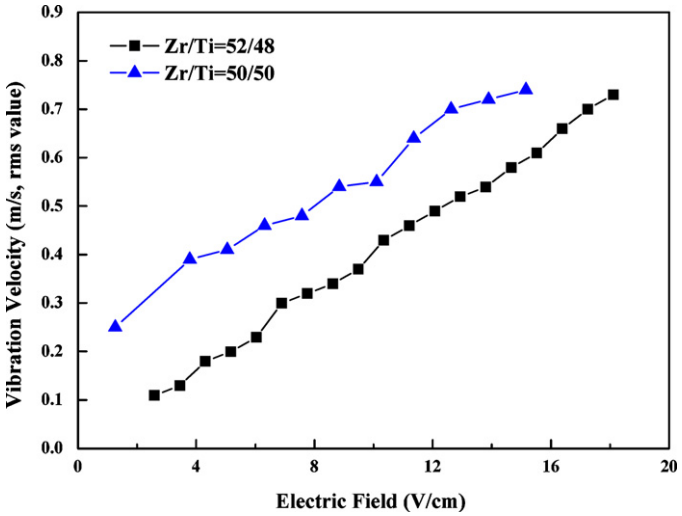

Fig. 8. Vibration velocity vs. electric field for PMgT–PMS–PZT ceramics.

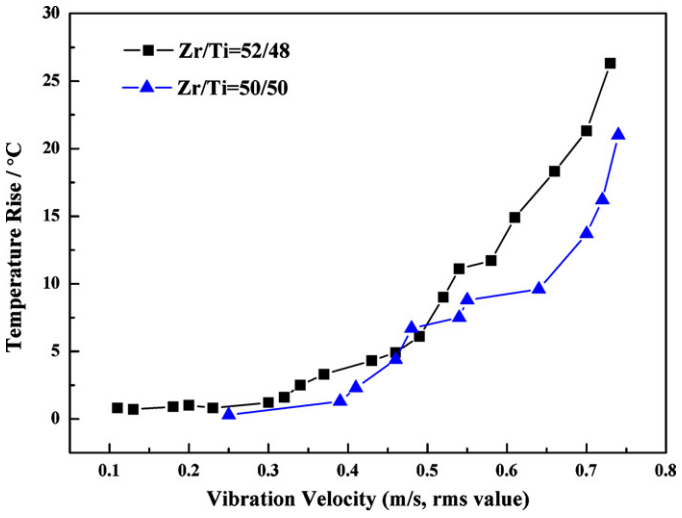

Fig. 9. Temperature rise vs. vibration velocity for PMgT–PMS–PZT ceramics.

velocity is defined as the velocity which produces a temperature rise of $\Delta T = 20\,^{\circ}C$ [29].

The relationship between temperature rise and the vibration velocity for the PMT–PMS–PZT ceramics with Zr/Ti = 52/48 and 50/50 is shown in Fig. 9. The sample with Zr/Ti = 50/50 produces much lower temperature rise than the sample of Zr/Ti = 52/48 under the same vibration velocity. The maximum vibration velocity ($\Delta T = 20\,^{\circ}C$) for the sample with Zr/Ti = 50/50 can reach as high as 0.74 m/s, which is much higher than conventional PZT ceramics driven under high power conditions, where υ_m is about to 0.3 m/s [29]. It is expected that this piezoelectric material can be utilized in high-power piezoelectric devices, such as ultrasonic motors.

According to Eq. (2), high Q_m benefits high υ_m. The Q_m of PMT–PMS–PZT ceramic with Zr/Ti = 50/50 is much higher than that of the ceramic with Zr/Ti = 52/48. Thus, much less heat and higher υ_m are generated in the former sample.

4. Conclusions

The effects of different Zr/Ti ratios on the structures, piezoelectric and dielectric properties of 0.05PMgT–0.05PMS–0.9PZT quaternary piezoelectric ceramics were discussed. The present results can be summarized as follows:

(1) A transition from rhombohedral phase to tetragonal phase was observed as the Zr/Ti ratio decreases in this system. The MPB of the ceramics was found near Zr/Ti = 48/52.
(2) The *P–E* loops of the ceramics present pinched shapes at low electric field and the distortions disappear at high electric fields because the pinning effect of defect dipoles can be fully overcome.
(3) The ceramics exhibits high piezoelectric and dielectric properties near the MPB. The optimum properties $\varepsilon_r = 817$, $d_{33} = 285$ pC/N, $k_p = 0.55$, $T_C = 302\,^{\circ}C$, $\tan\delta = 0.4\%$ and $Q_m = 1600$ were obtained at Zr/Ti = 50/50.
(4) Diffuse phase transition behavior was observed in PMgT–PMS–PZT ceramics according to the dielectric study. The exponent γ reaches its peak value at Zr/Ti = 50/50 due to the disorder phase structure near the MPB.
(5) The ceramics with Zr/Ti = 50/50 has a υ_m as high as 0.74 m/s, which is much higher than conventional PZT ceramics driven under high power conditions. It is expected that this piezoelectric material can be utilized in high-power piezoelectric devices, such as ultrasonic motors.

Acknowledgements

This study was financially supported by National Natural Science Foundation of China (50735002), Aeronautic Science foundation of China (2009ZC52042), NFSC-Guangdong Joint Fund (U0934004) and NUAA Research Funding No. NJ2010013.

References

[1] K. Kato, T. Sase, M. Chiba, Electron. Commun. Jpn. 83 (2000) 8–17.
[2] H.Y. Chen, X.B. Guo, Z.Y. Meng, Mater. Chem. Phys. 75 (2002) 202–206.
[3] S. Takahashi, S. Hirose, K. Uchino, J. Am. Ceram. Soc. 77 (1994) 2429.
[4] J. Yoo, Y. Lee, K. Yoon, S. Hwang, S. Suh, J. Kim, C. Yoo, Jpn. J. Appl. Phys. 40 (2001) 3256–3259.
[5] X. Zeng, X.Y. He, W.X. Cheng, X.S. Zheng, P.S. Qiu, J. Alloys Compd. 485 (2009) 843–847.
[6] C.C. Tsai, S.Y. Chu, C.K. Liang, J. Alloys Compd. 478 (2009) 516–522.
[7] X.L. Chao, D.F. Ma, R. Gu, Z.P. Yang, J. Alloys Compd. 491 (2010) 698–702.
[8] X.L. Chao, Z.P. Yang, Y.F. Chang, M.Y. Dong, J. Alloys Compd. 477 (2009) 243–249.
[9] H. Hao, S.J. Zhang, H.X. Liu, T.R. Shrout, J. Appl. Phys. 105 (2009) 024104.
[10] Z.G. Zhu, B.S. Li, G.R. Li, W.Z. Zhang, Q.R. Yin, Mater. Sci. Eng. B 117 (2005) 216–220.
[11] Q. Li, Y. Yang, D.D. Wan, Y. Cheng, M. Zha, Mater. Sci. Eng. B 163 (2009) 145–150.
[12] P.D. Gio, V.D. Dan, J. Alloys Compd. 449 (2008) 24–27.
[13] Z.G. Zhu, G.R. Li, B.S. Li, Q.R. Yin, K.L. Jiang, Ceram. Int. 34 (2008) 2067–2072.
[14] D.Y. Jeong, J. Ryu, D.S. Park, Mater. Sci. Eng. B 163 (2009) 88–92.
[15] K. Carl, K.H. Hardtl, Ferroelectrics 17 (1978) 473.
[16] G. Arlt, H. Neumann, Ferroelectrics 87 (1988) 109.
[17] M.H. Lente, J.A. Eiras, J. Appl. Phys. 92 (2002) 2112.
[18] H.B. Zhang, S.L. Jiang, Y.K. Zeng, Appl. Phys. Lett. 93 (2008) 192901.
[19] K. Carl, K.H. Hardtl, Phys. Stat. Solidi [a] 8 (1971) 87–91.
[20] D. Berlincourt, C. Cmolik, H. Jaffe, Proc. IRE 48 (1960) 220–229.
[21] C.H. Wang, Ceram. Int. 30 (2004) 605–611.
[22] S. Choudhury, L.Q. Chen, Y.L. Li, Appl. Phys. Lett. 91 (2007) 032902.
[23] C.M. Foster, G.R. Bai, R. Csencstis, J. Vetrone, R. Jammy, L.A. Wills, E. Carr, J. Amano, J. Appl. Phys. 81 (1997) 2349–2357.
[24] S.K. Mishra, D. Pandey, Philos. Mag. B 76 (1997) 227–240.
[25] T. Liu, Q.C. Sun, X.J. Zuo, Bull. Chin. Ceram. Soc. 2 (2003) 30–33.
[26] K. Uchino, S. Nomura, Ferroelectric Lett. 44 (1982) 55–61.
[27] N.N. Wu, Y.D. Hou, C. Wang, M.K. Zhu, X.M. Song, H. Yan, J. Appl. Phys. 105 (2009) 084107.
[28] B.S. Li, G.R. Li, W.Z. Zhang, A.L. Ding, Mater. Sci. Eng. B 121 (2005) 92–97.
[29] Y.K. Gao, Y.H. Chen, J.G. Ryu, K. Uchino, D. Viehland, Jpn. J. Appl. Phys. 40 (2001) 687–693.